The Effect of the Differential Rotation of Photospheric Magnetic Features on the Synoptic Frame of the Photospheric Magnetic Field

X. P. Zhao, J. T. Hoeksema and P. H. Scherrer
W. W. Hansen Experimental Physics Laboratory, Stanford University

Abstract

The effect of the advection of magnetic features on synoptic frames has been estimated and it shows that for the time interval ranging from 4 to 14 days the differential rotation of magnetic features accounts for most of the surface transport of photospheric magnetic fields. It is shown that both the 1996.08.27_19:12:30 synoptic frame with the effect of differential rotation included and the footpoint area and the neutral line calculated on the basis of the new synoptic frame differe slightly from that without differential rotation. To determine the improvement made by including the effect of magnetic features' differential rotation, more samples are needed to compare with observed coronal structures.

The 2004 AGU Fall Meeting, December 12 – (14) – 18, 2004, San Francisco

1. Introduction

To model the temporal variation of large coronal structures on the time scale of days or less, "synoptic frames" or "dynamic synoptic maps" of the radial photospheric magnetic field have been constructed as the proxy of the instataneous whole surface distribution of the photospheric magnetic field at specific instants of time (Zhao, Hoeksema and Scherrer, 1997; Harvey and Worden, 1998; Worden and Harvey, 2000). Using the synoptic frames as the input to coronal field models the temporal variation of the 1996 August boot-shaped coronal hole boundary on the time scale of a day and the temporal variation of the 1994 April Soft X ray arcade on the time scale of several hours (Zhao, Hoeksema and Scherrer, 1999; 2000) have been modeled.

The synoptic frame of the photospheric magnetic field at a specific instant of the time was constructed by inserting a remapped magnetogram at the specific time into a classical Carrington coordinate map with the central strip of the map corresponding to the Carrington longitude at the specific time (see Figure 1). However, the field in the part of the synoptic frame outside the inserted magnetogram are observed not in the same time as the specific time. The difference between the specific time and the time when magnetic features at pixels outside the inserted magnetogram were observed ranges from 4 days to 14 days. During the time interval, the field distribution can be changed due to the Sun's differential rotation, the meridianal flow, and the random walk diffusion as well as the emergence and cancellation of the magnetic flux.

The flux-transport equation of the photospheric magnetic field (e.g. Wang, Sheeley and Lean, 2000) that incorporates the effects of advection and diffusion has been used to produce the "instantaneous" maps from previous classical Carrington maps. Recently, a flux-dispersal model has been developed that assimilates SOHO/MDI magnetograms and acoustic far-side imanging into the flux-transport equation and successfully produces the instantaneous whole surface distribution of the radial magnetic field. (Schrijver and Derosa,

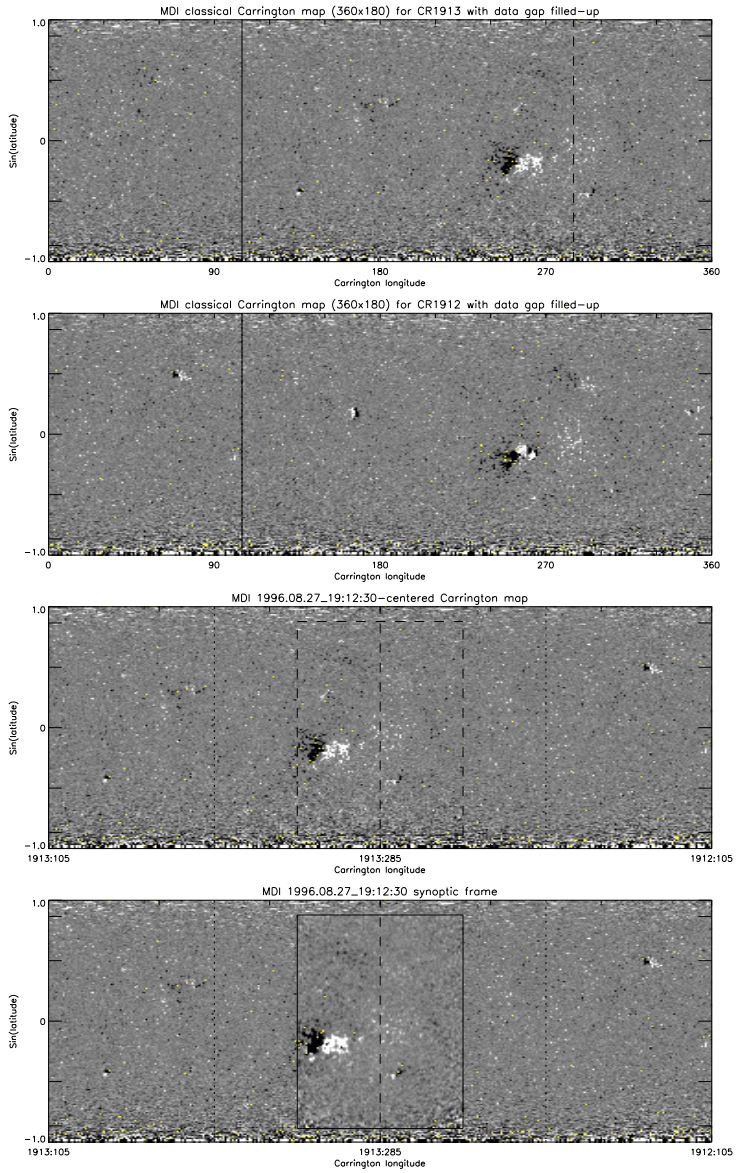

Fig. 1.— The construction of the date-centered Carrington map (the third panel) and synoptic frame (the fourth panel) on the basis of classical Carrington coordinate maps (the first and second panels) and the full-disk magnetogram (the central part of the synoptic frame boundered by solid lines)

2003 and references therein).

We plan to improve the synoptic frame by adding the effects of advection (differential rotation and meridinal flow) and acoustic far-side imanging into the part of a synoptic frame outside the inserted magntogram. To see if it is possible to improve the synoptic frame with a rather simple and direct procedure, this work studies the effect of the different rotation of photospheric magnetic features on the synoptic frames and on the predicted coronal holes and the base of the heliospheric current sheet near the sunspot minimum when new magnetic flux emerges rarely.

2. The effect of the advection on classical maps of large-scale field

We use the differential rotation law given by

$$\omega(\theta) = A + B\sin^2(\theta) + C\sin^4(\theta) \tag{1}$$

where $\omega(\theta)$ is the sidereal rotation rate, θ is the latitude, and coefficients are those fit by Snodgrass (1992): $A = 2.897$, $B = -0.339$, and $C = -0.485$ $\mu rads^{-1}$ for magnetic features. Snodgrass fit this law for latitudes within 50° of the solar equator. Deng, Wang and Harvey (1999), using magnetic tracers, found that the Snodgrass fit is adequate to first-order for solar rotation at polar latitudes.

Figure 2 displays such shifts of pixels' heliographic longitudes at different latitudes. For example, the pixel of a magnetic feature located at the latitude of 85° and Carrington longitude of 360° corresponding to t_{360} may be shifted to Carrington longitude of $\sim 300°$ at t_{180}. To fill up the gap due to the effect of the differential rotation at longitudes greater than 300° observational data corresponding to Carrington longitude of 60° in last Carrington rotation are needed (See red curves in Figure 2).

The Sun's meridinal circulation is slow, of order of $10ms^{-1}$. We use an approximation of the Wang and Sheeley (1994) meridinal flow model,

$$M(\theta) = 8|\sin\theta|^{0.3}|\cos\theta|^{0.1} \tag{2}$$

The peak poleward speed of $7.2ms^{-1}$ is reached at $\theta = 30°$ latitude in each hemisphere. Using the peak poleward speed and the bigest time difference of 14 days the maximum shift of the pixel's latitude is only 0.7°.

Thus for the first-order approximation, the effect of Sun's meridinal circulation in the time difference less than 15 days on classical maps may be neglected.

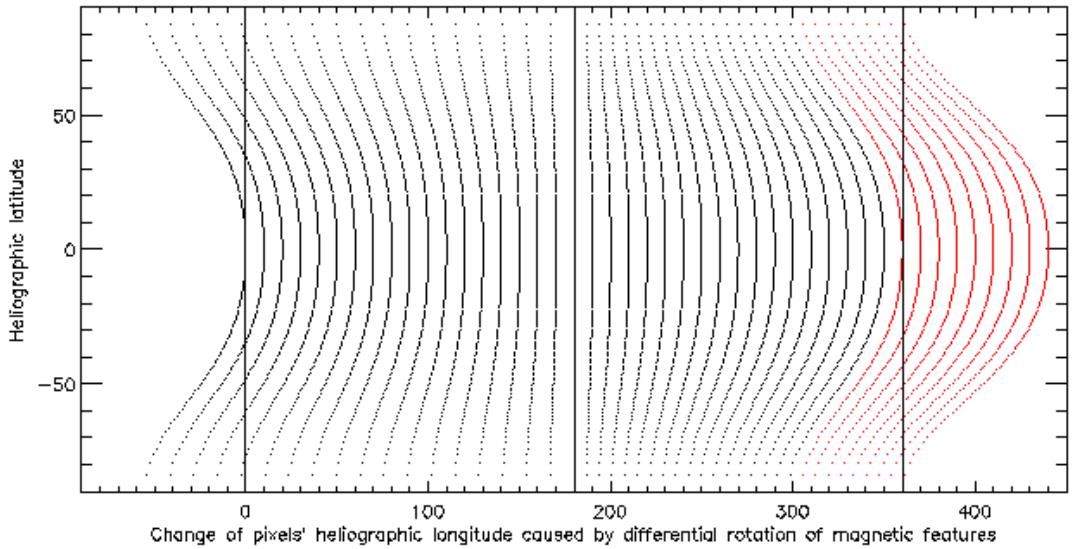

Fig. 2.— The changes of pixels' longitude due to the differential rotation of photospheric magnetic features

3. The synoptic frames without and with the effect of differential rotation

Figure 2 shows that because of the differential rotation of magnetic features the pixel distribution in the part with longitudes greater than 180° become concentrated with respect to the classical Carrington map and in the part with longitudes less than 180° become few and far between. Thus the flux over a unit area at a specific location wouold be the average of all fluxes moved into this unit area due to the pixels' moving around.

Figure 3 displays the 1996.08.27_19:12:30 centered Carrington map without differential rotation (the first panel), the 1996.08.27_19:12:30 centered Carrington map with differential rotation (the second panel), the 1996.08.27_19:12:30 synoptic frame without differential rotation (the third panel), and the 1996.08.27_19:12:30 synoptic frame with differential rotation (the fourth panel). The corresponding low-resolution polarity inverse lines (white curves) are overploted in each panel for showing the effect of the differential rotation on the field configuration (For example, the structures marked by 1, 2, 3, 4, 5, 6, 7, 8, 9, 10 between the first and second panels and the strucures marked by 11, 12, 13, 14 between the second and third panels).

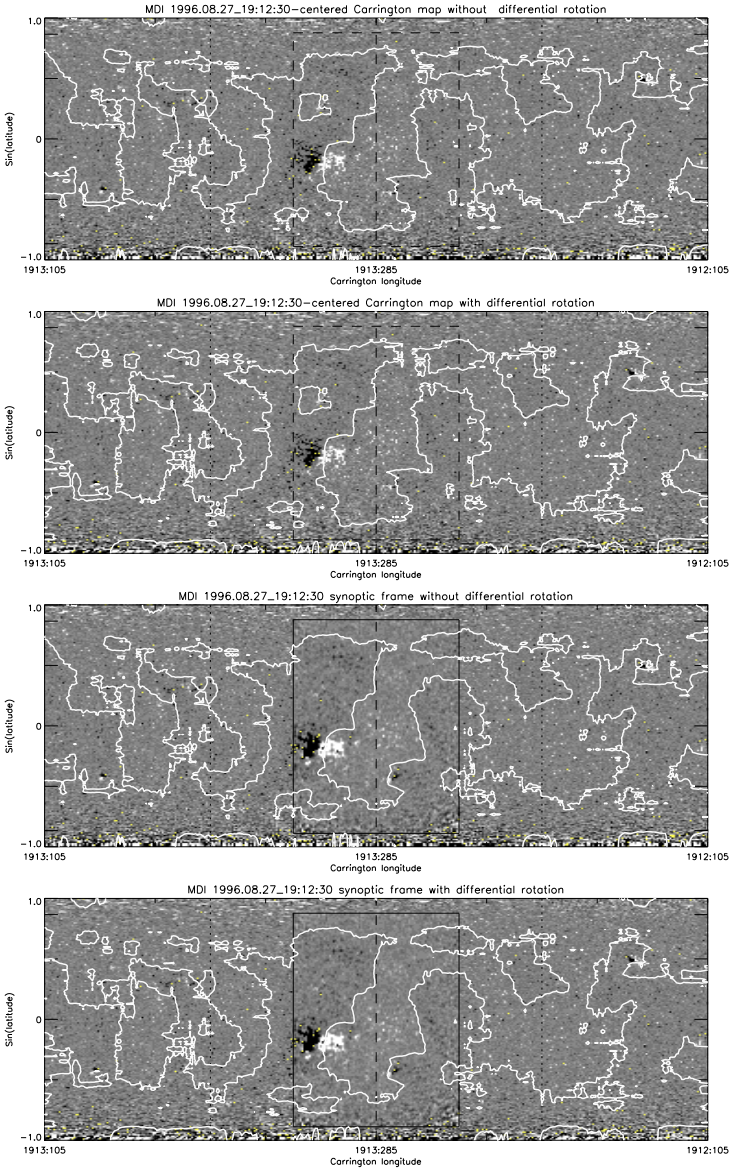

Fig. 3.— The four proxies of the whole surface distribution of the radial photospheric magnetic field.

4. The predicted coronal hole and HCS

Figure 4 shows the coronal holes and the base of the heliospheric current sheet calculated using the four proxies of the whole surface distribution of the photospheric magnetic field in Figure 3. The calculated positive (blue) coronal hole located near the Carrington longitude of 1913:285 in the fourth panel is slightly smaller that that in the third panel. The calculated neutral line in the fourth panel is shifted northward with respect to that in the third panel.

Figure 5 Compares the coronal holes cauclated using the 1996.08.27_19:12:30 synoptic frames without and with differential rotation and the potential field source surface model (the third and fourth panels) with the coronal holes observed using SOHO/EIT 19.5 nm and Kitt Peak He 1083.0 nm.

Figure 6 shows the outline of 1996.08.27_15:15 1083.0 nm hole and the over-ploted calculated footpoints of open field lines.

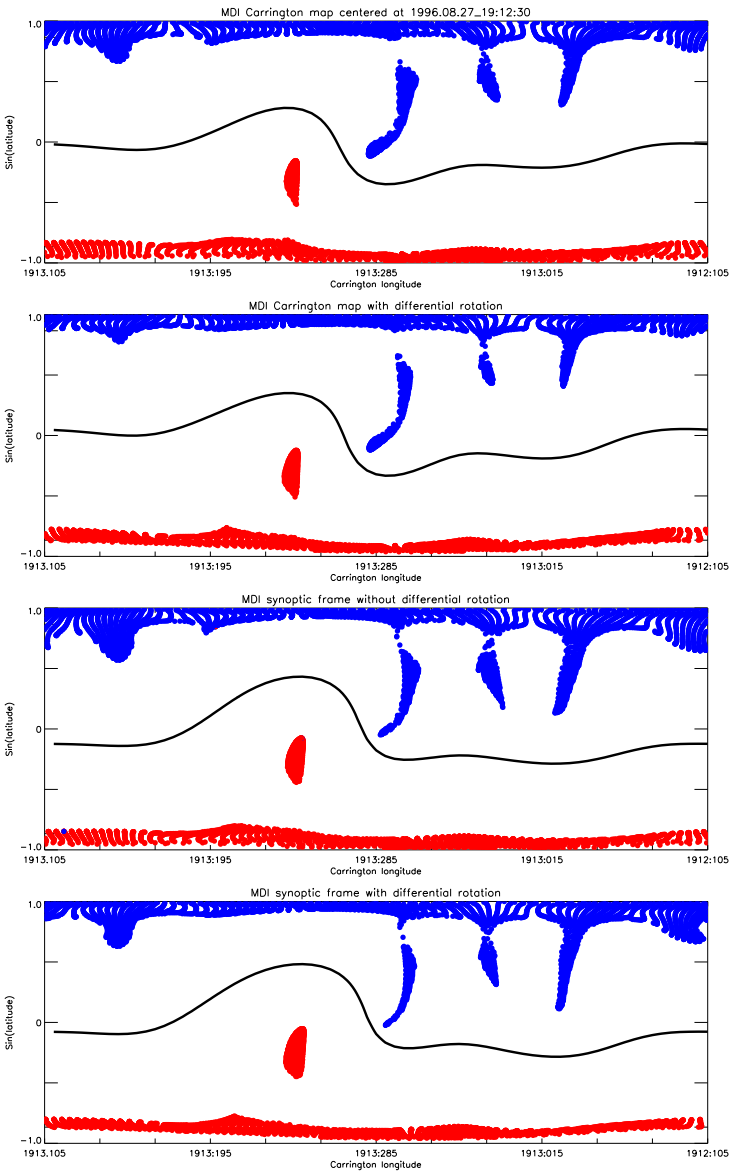

Fig. 4.— The neutral line and footpoint area of open field lines predicted using the four proxies of the whole surface distribution of the radial photospheric magnetic field in Figure 3.

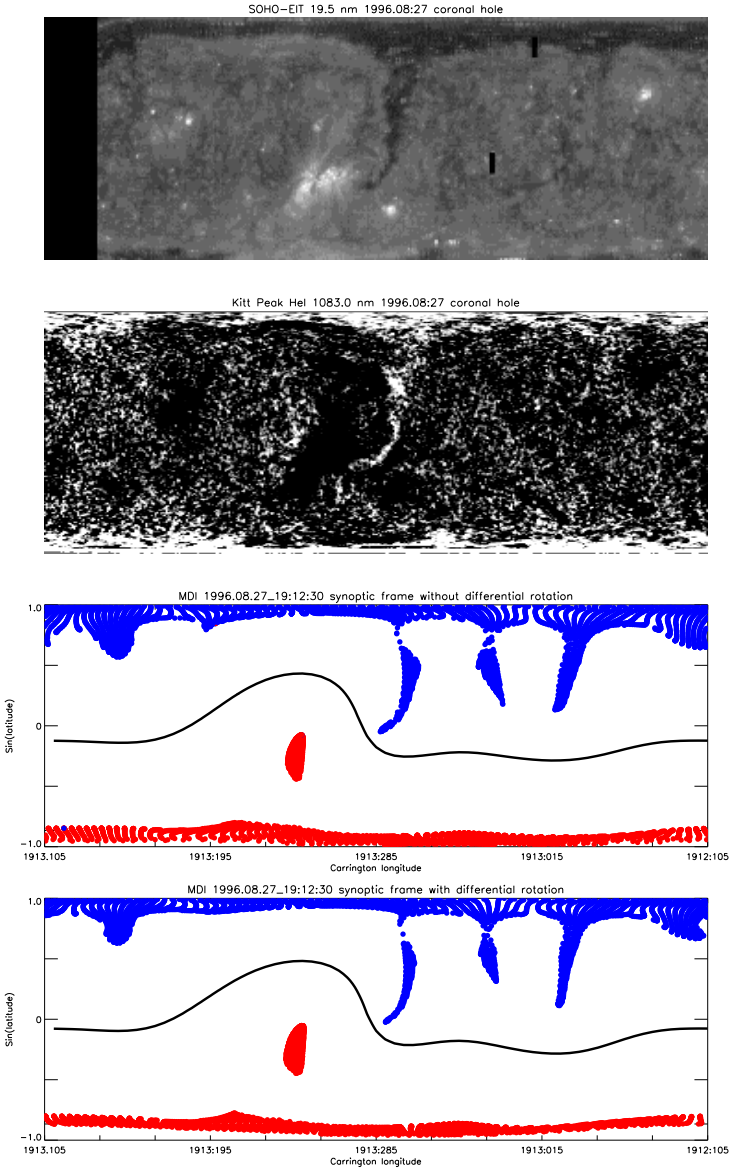

Fig. 5.— Comparison of coronal hole calculated using the 1996.08.27_19:12:30 synoptic frame without and with the effect of differential rotation with the 1996.08.27_15:15 coronal hole observed by SOHO/EIT 19.5 nm and KPNO He 1083.0 nm

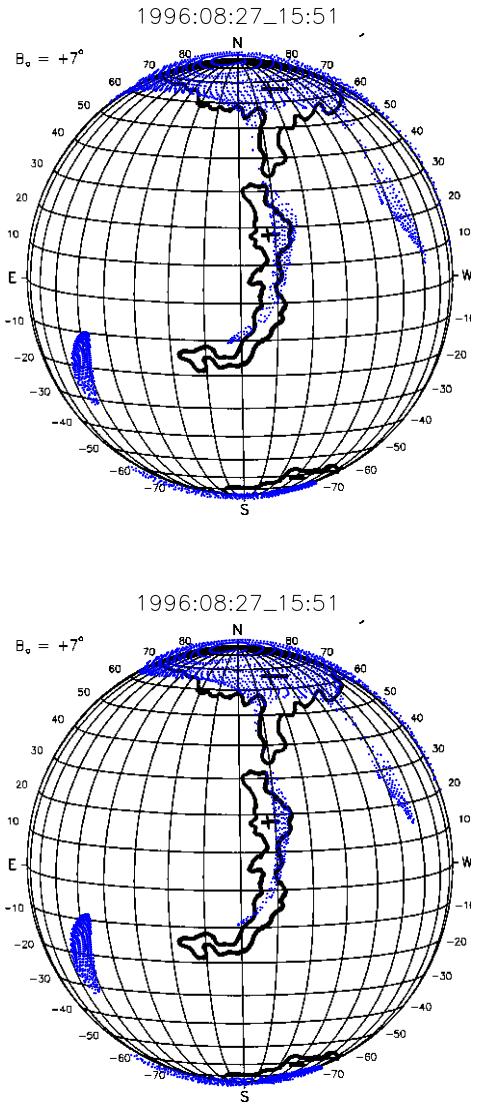

Fig. 6.— Comparison of coronal hole calculated using the 1996.08.27_19:12:30 synoptic frame without and with the effect of differential rotation with the outline of the 1996.08.27_15:15 coronal hole observed by KPNO He 1083.0 nm

5. Summary and Discussion

• Estimates show that for the time difference less than 14 days the differntial rotation of photospheric magnetic features accounts for most of the surface transport of magnetic fields.

• The surface transport of magnetic fields due to the differential rotation may cause slight change of the field configuration and field strength distribution for the 1997.08.27_19:12:30 synoptic frame.

• The neutral line and the footpoints of open field lines calculated using the new 1997.08.27_19:12:30 synoptic frame and the potential field source surface model slightly differ from what calculated using the synoptic frame without differential rotation.

• The predicted 1997.08.27 coronal holes calculated using the synoptic frames without and with differential rotation are compared with observed 1997.08.27 coronal hole. More samples are needed to determine whether or not the synoptic frames are improved after including the effect of the differential rotation of magnetic features.